Parameter Estimation in an SPDE Model for Cell Repolarisation*

Randolf Altmeyer†, Till Bretschneider‡, Josef Janák§, and Markus Reiß¶

Abstract. As a concrete setting where stochastic partial differential equations (SPDEs) are able to model real phenomena, we propose a stochastic Meinhardt model for cell repolarisation and study how parameter estimation techniques developed for simple linear SPDE models apply in this situation. We establish the existence of mild SPDE solutions and we investigate the impact of the driving noise process on pattern formation in the solution. We then pursue estimation of the diffusion term and show asymptotic normality for our estimator as the space resolution becomes finer. The finite sample performance is investigated for synthetic data resembling experimental findings for cell orientation.

Key words. Local measurements, stochastic partial differential equation, pattern formation, Meinhardt model, stochastic reaction-diffusion equation, drift estimation, augmented MLE

AMS subject classifications. Primary: 60H15, 92C37, 62M05; Secondary: 60J60.

1. Introduction.

Stochastic partial differential equations (SPDEs) generalize deterministic partial differential equations (PDEs) by introducing driving noise processes into the dynamics. These noise processes encapsulate unresolved and often unknown processes happening at faster scales and random external forces acting on the system. Not only the theory of SPDEs, but also the statistics for SPDEs have recently seen a significant development, paving the way for a realistic modeling of complex phenomena. We demonstrate the ability of SPDE models to describe cell repolarisation patterns and we show how parameter estimation techniques, developed for simplified linear models, apply in more complex and physically relevant situations. We see this as an important step to make theoretical tools also available for concrete experimental setups. For the sake of clarity we focus on a specific stochastic cell polarisation problem, but the methodology has a much broader scope.

The SPDE we are interested in belongs to a general class of activator-inhibitor models, which can be described by two coupled stochastic reaction-diffusion equations $X = (A, I)$ of the form

$$\begin{cases} \frac{\partial}{\partial t}A(t,x) = D_A \frac{\partial^2}{\partial x^2}A(t,x) + f_A(X(t,x),x) + \sigma_A \xi_A(t,x), \\ \frac{\partial}{\partial t}I(t,x) = D_I \frac{\partial^2}{\partial x^2}I(t,x) + f_I(X(t,x),x) + \sigma_I \xi_I(t,x), \end{cases} \tag{1.1}$$

*This research has been partially funded by Deutsche Forschungsgemeinschaft (DFG) - SFB1294/1 - 318763901.

†University of Cambridge, Department of Pure Mathematics & Mathematical Statistics, Wilberforce Road, CB3 0WB Cambridge, United Kingdom (ra591@cam.ac.uk).

‡Department of Computer Science, University of Warwick, Academic Loop Road, CV4 7AL Coventry, United Kingdom (T.Bretschneider@warwick.ac.uk).

§Universität Potsdam, Institut für Mathematik, Karl-Liebknecht-Str. 24/25, 14476 Potsdam, Germany(josefjanak@seznam.cz).

¶Humboldt-Universität zu Berlin, Institut für Mathematik, Unter den Linden 6, 10099 Berlin, Germany (mreiss@math.hu-berlin.de).

where $X = (A, I)$, with nonlinear functions f_A, f_I and with space-time white noise processes ξ_A, ξ_I. In cell dynamics, we think of A as a hypothetical signalling molecule that in response to an external signal gradient becomes enriched on one side of the cell, yielding polarity. I counter-acts A so that removal of the signal results in loss of polarity. We here specifically consider repolarisation, where the extracellular signal gradient is inverted so that A is removed from one side of the cell and reappears on the opposite side, cf. Figure 1 below.

In directed animal cell motion cells respond to for example chemical or mechanical extracellular signal gradients by adopting a functional asymmetry in form of a front-rear pattern. Protrusion of the cell front is driven by local oriented growth of a dense network of cytoskeletal actin filaments pushing the cellular envelope [29]. Myosin-II motor molecules contracting the looser, ubiquitous cortical actin network lining the cell membrane result in retraction of the cell rear in stringent environments [11].

Models for spontaneous symmetry breaking in non-linear reaction diffusion systems by Turing [34] have been instrumental in understanding biological pattern formation, often paraphrased in form of simple deterministic two-variable activator-inhibitor models such as (1.1) without noise terms. Suprathreshold random perturbations can result in fast autocatalytic local growth of the activator variable A, which eventually is kept in check by the slower inhibitor I. Faster diffusion of the inhibitor compared to the activator prevents formation of nearby activator peaks.

Meinhardt [27] has been the first to apply such models to cell polarisation in the context of cell migration, where the ratio of activator-inhibitor diffusion can be tuned to either obtain a single stable cell front (Figure 1(center)), or multiple independent fronts associated with non-directed random cell motility. Various mathematical models for cell polarisation and gradient sensing have been postulated ([21], [30], [19]) aiming to capture different aspects of cellular physiology for example with regards to adaptation to extracellular signals, reviewed in [6]. [24] fitted deterministic versions of three different models for cell polarisation to experimental data of cells in a microfluidic chamber responding to inversion of gradients of hydrodynamic shear flow of different strengths [13]. The parameter calibration was based on a least-squares ansatz, implicitly assuming that the deterministic dynamics are corrupted by Gaussian measurement noise.

Recognising that in confined spaces and with limited number of molecules noise becomes increasingly important, more recently stochastic reaction-diffusion models for different biological problems have been employed, e.g. in [2], [33]. Spontaneous symmetry breaking in Turing-type models requires initial random perturbations, but we expect dynamic noise to destabilise patterns if the power of the noise is too large.

In the current paper we present a stochastic version of the modified Meinhardt two-variable model [24]. We believe that the stochasticity in the data is to some considerable extent due to dynamic noise entering the dynamics as in (1.1). The data generated from such a stochastic Meinhardt model is qualitatively of a different nature compared to a deterministic PDE model corrupted by measurement errors. We perform a systematic study of the effect of different noise levels on the repolarisation of cells. One result is that inclusion of moderate levels of noise in the model speeds up the repolarisation of cells, which biologically is interesting because it seems to be against our intuition that noise

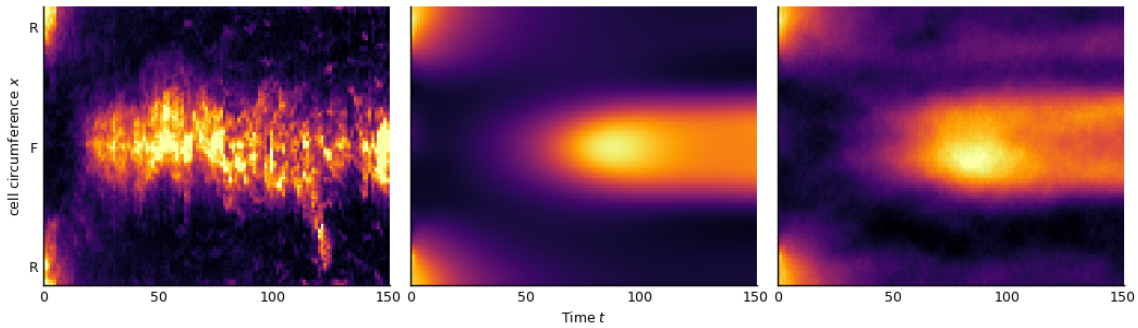

Figure 1: Heat maps for the space-time evolution of the activator A, brighter colors mean higher values, space region R denotes the old front/new rear, region F is the new front/old rear; (left) experimental data for measured fluorescence values averaged over several *Dictyostelium* cells reacting to a gradient of shear flow; (center) solution to the deterministic Meinhardt model with the same initial condition, (right) a typical realisation of the stochastic Meinhardt model with noise level 0.02.

would negatively interfere with the formation of a pattern.

Recently, new tools for parameter estimation of stochastic differential equations have been developed, see [8] for an overview. Most approaches focus on estimating coefficients for the linear part of the equation, either from discrete [9], [16] or spectral [17], [32] observations, but also aspects of the driving noise have been analysed [7], [5]. Owing to the physical restriction of being able to measure only local averages, [4] have introduced local measurements and constructed estimators in a linear SPDE for the diffusion term which are provably rate-optimal. Even more, the proposed estimators apply in a nonparametric setting of spatially varying diffusion and are robust to misspecification of the noise or when subject to certain nonlinearities [3].

We extend the estimation method in [4] to cope also with multiple spatial measurements, systems of SPDEs as (1.1) and with more general boundary conditions (here periodic boundary conditions will apply). We shall perform parameter estimation in the stochastic Meinhardt model for cell repolarisation and provide confidence intervals to quantify the uncertainty. In particular, we are interested in determining the diffusion constant for the activator in the Meinhardt model. Although the activator variable in the model cannot be directly related to a specific molecular component, putting limits on how fast the activator spreads can ideally help narrowing down possible mechanisms. For example, spreading of the activator could be down to lateral growth of the actin network (slow), diffusion of chemoattractant receptors within the cell membrane (medium) or diffusion of phospholipid signalling molecules (PIP3) within the cell membrane (fast).

Mathematically, we derive a central limit theorem for our estimator by using advanced tools from stochastic analysis and semigroup theory. We are aware of only one related work [31] which uses the spectral method to fit parameters of a 2D Fitz-Hugh-Nagumo model for travelling actin waves through cells. For the stochastic Meinhardt model we compare in Section 5 below our method with the spectral estimation method.

In the next Section 2 the stochastic Meinhardt model is introduced, along with a rigorous proof for existence of a solution. Section 3 presents the main insights how adding noise to the Meinhardt model affects the dynamics and repolarisation. In Section 4 estimators for local measurements of the activator are analysed mathematically and applied in Section 5 to synthetic data. Section 6 discusses the main results. All technical details and proofs are deferred to Appendix A. A description of the setup for numerical experiments based on the fitted parameter values from [24] can be found in Appendix B.

2. The stochastic Meinhardt model. Diffusion is considered to take place along the cell contour, and so we study the equation (1.1) for $t \geqslant 0$ on a circle Λ of length $L > 0$ or equivalently on $\Lambda = [0, L]$ with periodic boundary conditions. We think of A as a large, membrane-bound autocatalytic activator requiring f_A to be nonlinear and with slow diffusion (that is, small D_A). The production of A is counteracted by a small cytosolic inhibitor I with faster diffusion (that is, $D_I > D_A$), where f_I is linear or nonlinear. In case of the two-variable Meinhardt model the functions f_A and f_I are given by

$$f_A(y,x) = r_A \frac{s(x)\left(b_A + y_1^2\right)}{\left(s_I + |y_2|\right)\left(1 + s_A y_1^2\right)} - r_A y_1, \quad f_I(y,x) = b_I y_1 - r_I y_2, \tag{2.1}$$

for $y \in \mathbb{R}^2$ and $x \in \Lambda$. The function

$$s(x) = 1 + a \cdot \cos(2\pi(x/L + 1/2)) \tag{2.2}$$

corresponds to an extracellular signal, for example a gradient of chemoattractant, which stimulates the production of A with signal strength modulated by a constant a. The constants r_A, r_I and b_A, b_I are degradation and production rates, s_A controls the saturation and the Michaelis-Menten constant s_I prevents f_A from exploding. While b_I is fixed in our setup, it will generally depend on the pressure of the signal s [24]. For a more detailed description of the nonlinearities f_A, f_I and a stability analysis for varying parameters see [23], [28].

Additional external forces acting on the cell membrane are modeled by two independent space-time white noise processes ξ_A, ξ_I. By space-time white noise we mean a centered Gaussian process ξ on $[0,T] \times \Lambda$ with covariance function

$$\operatorname{Cov}\left(\xi(t,x), \xi(t',x')\right) = \delta(t-t')\delta(x-x').$$

By integrating formally against test functions, ξ induces an isonormal Gaussian process on $L^2([0,T] \times \Lambda)$. In this way, space-time white noise corresponds to a random Schwartz distribution on $L^2(\Lambda)$ with values in negative Sobolev spaces [15]. Since the nonlinearity $f_A(X(t,x),x)$ is not well-defined for a distribution valued process X, this means we cannot obtain classical solutions to the SPDE (1.1). After formally integrating the noise, however, $W(t) = \int_0^t \xi(s,\cdot)ds$ is a (cylindrical) Wiener process with values in $L^2(\Lambda)$ [12], and we can use the well-developed theory for SPDEs to show that (1.1) is well-posed in the mild sense. The solution even has some minimal spatial regularity.

Theorem 2.1. *Consider the stochastic Meinhardt model corresponding to the SPDE in (1.1) with nonlinearities f_A, f_I from (2.1) on $\Lambda = [0,L]$ with periodic boundary conditions.*

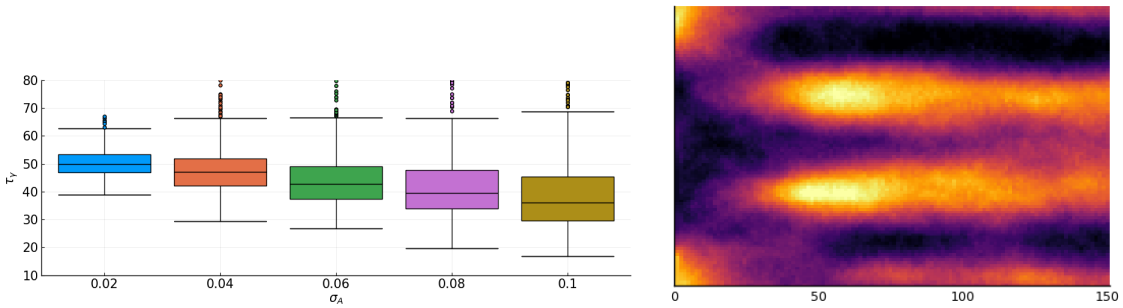

Figure 2: (left) Boxplots for the distribution of the time to repolarisation τ_γ for different noise levels σ_A; (right) a typical realisation of the stochastic Meinhardt model with larger noise level 0.05.

Assume for the initial value $(A_0, I_0) \in C^{2+s}(\Lambda; \mathbb{R}^2)$ *for* $0 < s < 1/2$. *Then there exists a unique mild solution* $X = (A, I) \in C([0, T]; C^s(\Lambda; \mathbb{R}^2))$.

For the proof in Appendix A.1 we shall employ the language of stochastic analysis, while for modeling purposes we prefer (1.1) with the physical white noise interpretation. A more realistic model might consider multiplicative noise levels σ_A, σ_I depending on X. Moreover, also the parameters and initial conditions could be subject to noise [19]. Here, we refrain from this generality and focus on the impact of simple additive space-time white noise in (1.1). Note that neither the model proposed by Meinhardt nor other models suggested in the literature for cell repolarisation include dynamic noise so far.

3. The effect of noise. In Turing-type models for pattern formation noise in the initial condition is required to leave a homogeneous steady state. Its strength determines how fast a suprathreshold level for the activator A starts growing into a pattern whose wavelength can be determined by linear stability analysis. Dynamic noise, on the other hand, is expected to destabilise this pattern either over time, or very suddenly. Contrary to this intuition, we will now describe two noteworthy effects arising from moderate noise levels.

Noise speeds up repolarisation. In Figure 1(center) we see the solution of (1.1) starting from a polarised state with high activator concentration in some part of the cell called 'rear'. Stimulated by the extracellular signal (2.2) the activator breaks down in order to reappear in an area of high signal strength called 'front', and the cell repolarises. Figure 1(right), on the other hand, contains a typical realisation of the SPDE (1.1). The evolution of activator concentration deviates considerably from the deterministic dynamics, but repolarisation is still achieved. For a more quantitative analysis consider the relative activator concentrations

$$\mu_F(t) = \frac{1}{L}\int_{S_F} A(t,x)dx, \qquad \mu_R(t) = \frac{1}{L}\int_{S_R} A(t,x)dx, \qquad t \geqslant 0,$$

near the front $S_F = [L/4, 3L/4]$ and the rear $S_R = [0, L/4) \cup (3L/4, L]$. With this we define the 'time to repolarisation'

$$\tau_\gamma = \inf\{t \geqslant 0 : \ \mu_F(t) \geqslant \gamma \mu_R(t)\}$$

as the time when the activator concentration in the front part is significantly higher than in the rear depending on a threshold $\gamma > 1$. We computed τ_γ for 500 Monte Carlo iterations with $\gamma = 1.2$ for different noise levels $\sigma_A \in \{0.02, 0.04, \dots, 0.10\}$ (see Appendix B for details on the numerical setup). The corresponding boxplots describing the distribution of τ_γ depending on σ_A is contained in Figure 2(left). We see that the mean of τ_γ decreases for growing σ_A, while the variance increases. For example, while $\tau_\gamma = 50.82$ in the deterministic case (i.e., $\sigma_A = 0$), it is $\tau_\gamma = 40.12$ (on average) in the case $\sigma_A = 0.10$. A similar behaviour holds for varying σ_I. The same qualitative results were obtained for parameters and initial conditions different from the ones in Appendix B.

We can conclude that repolarisation is not only stable under noise, but it is even accelerated. The interpretation of this behaviour could be that the noise breaks symmetries, making the dynamics more 'turbulent' and therefore the creation of a new front is sped up.

In principle, the noise may act such that repolarisation is never achieved. In case of the noise levels for σ_A considered above, however, this was not an issue and only very few realisations of X had to be discarded for computing τ_γ. Moreover, realisations of (1.1), which would have lead to negative concentrations of A or I, were not taken into account (even for $\sigma_A = 0.1$ this concerned only 2.6% of all simulated paths).

Splitting of the front. For the deterministic Meinhardt model it has been shown by [23] that the repolarised front may not be stable. Indeed, if the parameters, obtained from fitting data on the short timescales at which repolarisation typically occurs (120 sec), are used for long term simulations, then the front splits into several parts. This can be verified for the parameters in Appendix B: upon repolarisation, the front splits first into two parts (around time $t = 200$) and then into three parts (around time $t = 700$).

From Figure 2(right) we see, however, that the stochastic Meinhardt model with a larger noise level may lead to a sudden split into several fronts, and even a renewed polarisation of the rear. For very small noise levels (for example, $\sigma_A = 0.01$) the front splitting into three fronts occurs much faster (around $t = 400$ - 500 s) than in the deterministic system, while for larger noise levels this occurs even faster.

We want to note that front splitting is a common feature of amoeboid cell migration, allowing cells to explore their environment. It is visible in single cell data [24], but not in Figure 1(left), which corresponds to data averaged over several cells. Still, in strong signal gradients cells can move with a single front for long times (>10 minutes) [24]. The Meinhardt model for long term simulations requires a smaller diffusivity D_I. When D_I was reduced by 25%, both deterministic and stochastic solutions produced a single stable front.

4. Parameter estimation. We derive an estimator $\hat{D}_{A,\delta}$ of the diffusivity D_A from first principles and state its main properties. Let us assume that we can measure the activator A at M points $x_k \in \Lambda$ for $k = 1, \dots, M$ over a period of time $[0, T]$. Measurements usually correspond to fluorescence distributions (for example of actin in [24]) at the cell cortex and are obtained through microscopy. This means that every measurement necessarily has a minimal spatial resolution $\delta > 0$ determined by the experimental setup. It can be described by a *local measurement* [4], that is, a linear functional

$$A_\delta(t, x_k) := \langle A(t), K_{\delta,x_k} \rangle = A(t) * K_{\delta,\cdot}(x_k), \quad 0 \leqslant t \leqslant T, \tag{4.1}$$

where $\langle \cdot, \cdot \rangle$ denotes the $L^2(\Lambda)$ inner product and $*$ means convolution with respect to $K_{\delta,x_k}(x) := \delta^{-1/2} K(\delta^{-1}(x - x_k))$ for a compactly supported function $K \in H^2(\mathbb{R})$, the classical L^2-Sobolev space of order 2. K_{δ,x_k} corresponds to the point spread function in imaging systems. A particular example for K is the standard bump function (see Section 5 below). The scaling by $\delta^{-1/2}$ is irrelevant for the estimator, but normalizes K_{δ,x_k} in L^2-norm and eases the notation later. From (1.1) we find that $A_\delta(t, x_k)$ satisfies

$$\frac{\partial}{\partial t} A_\delta(t, x_k) = D_A A_\delta^\Delta(t, x_k) + \langle f_A(X(t, \cdot), \cdot), K_{\delta,x_k} \rangle + \sigma_A \|K_{\delta,x_k}\| \, \xi_{A,k}(t), \tag{4.2}$$

with scalar white noise (in time) $\xi_{A,k}(t) = \langle \xi_A(t), K_{\delta,x_k} \rangle / \|K_{\delta,x_k}\|$, and where

$$A_\delta^\Delta(t, x_k) := \frac{\partial^2}{\partial x^2} A_\delta(t, \cdot)\big|_{x=x_k} = \Big\langle A(t), \frac{\partial^2}{\partial x^2} K_{\delta,x_k} \Big\rangle. \tag{4.3}$$

Neglecting the contribution of the nonlinear term in (4.2) leads to a parametric estimation problem for D_A with respect to the scalar processes $(A_\delta(t, x_k))_{0 \leqslant t \leqslant T}$ for $k = 1, \dots, M$. The maximum-likelihood estimator can be obtained, in principle, by Girsanov's theorem [22], but this leads to a non-explicit filtering problem, as explained in [4] for the case $M = 1$. Instead, consider the modified likelihood with stochastic differentials $dA_\delta(t, x_k)$ (in time)

$$\mathcal{L}_\delta(D_A) = \exp\left(\frac{D_A}{\sigma_A^2 \|K_{\delta,x_k}\|^2} \sum_{k=1}^M \left(\int_0^T A_\delta^\Delta(t, x_k) dA_\delta(t, x_k) - \frac{D_A}{2} \int_0^T \left(A_\delta^\Delta(t, x_k) \right)^2 dt \right) \right).$$

Maximising with respect to D_A and assuming that we have also measurements $(A_\delta^\Delta(t, x_k))_{0 \leqslant t \leqslant T}$ at our disposal, leads to the *augmented MLE*

$$\hat{D}_{A,\delta} = \frac{\sum_{k=1}^M \int_0^T A_\delta^\Delta(t, x_k) dA_\delta(t, x_k)}{\sum_{k=1}^M \int_0^T (A_\delta^\Delta(t, x_k))^2 dt}. \tag{4.4}$$

Note that this extends the construction of [4] to more than one pair of local measurements. Equivalently, $\hat{D}_{A,\delta}$ can be obtained formally (that is, neglecting the term independent of D_A in the quadratic expansion and interpreting $\frac{\partial}{\partial t} A_\delta dt = dA_\delta$) as minimiser of the least squares contrast

$$D_A \mapsto \sum_{k=1}^M \int_0^T \left(\tfrac{\partial}{\partial t} A_\delta(t, x_k) - D_A A_\delta^\Delta(t, x_k) \right)^2 dt.$$

With Brownian motions $W_k(t) = \int_0^t \xi_{A,k}(s)ds$ we obtain from (4.2) the basic error decomposition

$$\hat{D}_{A,\delta} = D_A + \mathcal{I}_\delta^{-1} R_\delta + \sigma_A \|K_{\delta,x_k}\| \mathcal{I}_\delta^{-1} M_\delta, \tag{4.5}$$

$$\text{with} \quad \mathcal{I}_\delta = \sum_{k=1}^{M} \int_0^T \left(A_\delta^\Delta(t,x_k)\right)^2 dt, \qquad \text{(observed Fisher information)}$$

$$M_\delta = \sum_{k=1}^{M} \int_0^T A_\delta^\Delta(t,x_k) dW_k(t), \qquad \text{(martingale part)}$$

$$R_\delta = \sum_{k=1}^{M} \int_0^T A_\delta^\Delta(t,x_k) \langle f_A(X(t,\cdot),\cdot), K_{\delta,x_k}\rangle dt. \qquad \text{(nonlinear bias)}$$

For $M = 1$ and linear SPDEs with Dirichlet boundary conditions [4] show that $\mathcal{I}_\delta \to \infty$ in probability for resolution $\delta \to 0$. We will see that this remains true in the present case with periodic boundary conditions and fixed M. For independent Brownian motions W_k, for example when the K_{δ,x_k} have disjoint supports, the observed Fisher information $\mathcal{I}_\delta$ corresponds to the quadratic variation of the martingale part M_δ. Consistency of $\hat{D}_{A,\delta}$ is therefore expected to hold as soon as the nonlinear bias is not too large. For a nonlinearity depending only on the underlying process, that is A, [3] prove that this depends on its spatial regularity, but in our case $f_A(X(t,\cdot),\cdot)$ also depends on additional randomness through the inhibitor I.

We prove in Appendix A.2 for fixed T and M that $\hat{D}_{A,\delta}$ is not only a consistent estimator of D_A for resolution levels $\delta \to 0$, but also that its error satisfies a CLT with rate δ (which is optimal already for the linear case in [4]) and with explicit asymptotic variance.

Theorem 4.1. *Consider the setting of Theorem 2.1 and let $K \in H^2(\mathbb{R})$ have compact support such that $\|\frac{\partial}{\partial x} K\|_{L^2(\mathbb{R})} \neq 0$. If $\sigma_A > 0$, then, as $\delta \to 0$, $\hat{D}_{A,\delta}$ is a consistent and asymptotically normal estimator of D_A, that is,*

$$\delta^{-1}\left(\hat{D}_{A,\delta} - D_A\right) \xrightarrow{d} N\left(0, D_A \frac{\Sigma}{MT}\right), \quad \Sigma = \frac{2\|K\|_{L^2(\mathbb{R})}^2}{\|\frac{\partial}{\partial x} K\|_{L^2(\mathbb{R})}^2}.$$

The proof in Appendix A.2 is self-contained and significantly shorter compared to similar results in [4], [3]. The proof is also not restricted to Dirichlet or periodic boundary conditions. The asymptotic variance in Theorem 4.1 improves for more observations M and for a growing time horizon T, but is independent of the noise level σ_A and the nonlinearity f_A. This robustness is particularly important in modelling realistic nonlinear dynamics such as (1.1), which are subject to model uncertainties in parameters and even the form of the equation.

Remark 4.2. It is interesting to note that the robustness of the estimator $\hat{D}_{A,\delta}$ to nonlinear perturbations f_A is an impact of the driving noise process. If there is no noise, that is $\sigma_A = \sigma_I = 0$, then $A(t) \in C^2(\Lambda)$, $f_A(X(t,\cdot),\cdot) \in C(\Lambda)$ by classical theory for parabolic

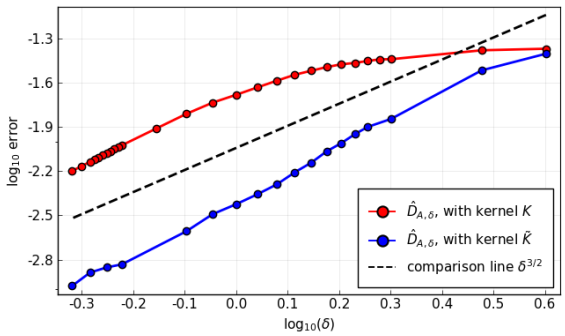

Figure 3: $\log_{10}$-$\log_{10}$ plot of root mean squared estimation errors for $M = \delta^{-1}$ and two different kernels.

PDEs [14] or argue as in the proof of Theorem 2.1, which does not assume nonvanishing noise. This implies by convolution approximation uniformly in $0 \leqslant t \leqslant T$ as $\delta \to 0$

$$\langle f_A(X(t,\cdot),\cdot), \delta^{-1/2} K_{\delta,x_k} \rangle \to f_A(X(t,x_k),x_k) \int_{\mathbb{R}} K(x)dx,$$
$$\delta^{-1/2} A^{\Delta}_{\delta}(t,x_k) = \left\langle \frac{\partial^2}{\partial x^2} A(t), \delta^{-1/2} K_{\delta,x_k} \right\rangle \to \frac{\partial^2}{\partial x^2} A(t,x_k) \int_{\mathbb{R}} K(x)dx.$$

From this and the basic error decomposition (4.5) it follows then, assuming $\int_{\mathbb{R}} K(x)dx \neq 0$ and $\frac{\partial^2}{\partial x^2} A(t,x_k) \neq 0$ for at least on x_k, that $\hat{D}_{A,\delta} - D_A$ converges to a non-zero constant. On the other hand, in the linear PDE case with $f_A \equiv 0$ we have exactly $\hat{D}_{A,\delta} = D_A$ and there is no estimation error.

As consequence of Theorem 4.1 we can easily construct an asymptotic confidence interval for D_A.

Corollary 4.3. *Consider the setting of Theorem 4.1. For $0 < \alpha < 1$ a confidence interval $I_{1-\alpha}$ for D_A with asymptotic coverage $1-\alpha$ as $\delta \to 0$ is given by*

$$I_{1-\alpha} = \left[\hat{D}_{A,\delta} - \frac{\delta}{(MT)^{1/2}} \left(\hat{D}_{A,\delta} \Sigma \right)^{1/2} q_{1-\alpha/2}, \hat{D}_{A,\delta} + \frac{\delta}{(MT)^{1/2}} \left(\hat{D}_{A,\delta} \Sigma \right)^{1/2} q_{1-\alpha/2} \right]$$

with the standard normal $(1-\alpha/2)$-quantile $q_{1-\alpha/2}$.

5. Application to synthetic data. Let us apply the results of the previous section to the estimation of the diffusion constant D_A. Synthetic data of local measurements are obtained by simulating the SPDE (1.1) using a finite difference scheme as explained in Appendix B with experimentally calibrated $D_A = 4.415 \times 10^{-2}$ for $m = 35 * L = 700$ points in space and $n = 35^2 * T$ points in time. As a typical example for the kernel K we use a standard bump function

$$K(x) = \exp\left(-\frac{10}{1-x^2} \right) \mathbf{1}_{[-1,1]}(x), \quad x \in \mathbb{R}, \tag{5.1}$$

but we also consider another kernel $\tilde{K} = \partial^2 K/\partial x^2$ for comparison. Note that $\tilde{K}$ oscillates more than K, and so we expect smaller estimation errors for $\tilde{K}$ according to Theorem 4.1. For different resolutions δ we let $M \equiv M(\delta) = \delta^{-1}$ and compute for each of the two kernels local measurements $A_\delta(t, x_k)$, $A_\delta^\Delta(t, x_k)$ according to (4.1) and (4.3) on a regular grid $x_k = Lk/M$, $k = 0, \dots, M-1$.

Figure 3 shows a $\log_{10}$-$\log_{10}$ plot of root mean squared estimation errors with respect to the augmented MLE $\hat{D}_{A,\delta}$, obtained after 1000 Monte Carlo iterations. We see that for small δ, the errors decay approximately like $\delta/\sqrt{M} = \delta^{3/2}$, as predicted by Theorem 4.1. This is true for both kernels, K and $\tilde{K}$, but the errors are significantly smaller for $\tilde{K}$. The observed difference in $\log_{10}$ errors is approximatly $0.65 \approx \log_{10}(0.0173) - \log_{10}(0.039)$ and corresponds to the reduced asymptotic variance in Theorem 4.1 with $\Sigma = 0.173$ for K and $\Sigma = 0.039$ for $\tilde{K}$.

We have verified the confidence intervals of Corollary 4.3 empirically for estimation with $M = 1$ at 100 different x_k in (4.4) and with kernel $\tilde{K}$. For $\delta = 0.013$ and at most points the coverage of the asymptotic 90%-confidence intervals $\mathcal{I}_{0.90}$ was near the nominal level, but the results were not homogeneous in space, with coverage dropping significantly at some points. This is due to the relatively large nonlinearity f_A in (4.2), where repolarisation leads to fast changes in the activator A (cf. Figure 1). This effect becomes smaller as $\delta \to 0$, as the nonlinearity plays no role in the asymptotic error according to Theorem 4.1.

Further unreported simulations show similarly good performance for the proxy MLE from [4], extended to M measurements as $\hat{D}_{A,\delta}$, at least with kernel $\tilde{K}$, with the estimation error differing from $\hat{D}_{A,\delta}$ by a constant factor (it almost coincides with $\hat{D}_{A,\delta}$ for kernel K). The spectral estimator [17], on the other hand, which is based on globally averaged observations instead of local information, was significantly affected by the large nonlinear dynamics, and did not perform well. This is in line with similar findings by [31] in a related application to cell motility. This suggests that the augmented MLE is able to compensate for local disturbances (like traveling waves) better than the spectral estimator.

6. Discussion. We have extended parameter estimation methods developed for linear SPDEs to systems of stochastic-reaction diffusion equations with periodic boundary conditions. The inclusion of noise into biological models is becoming increasingly relevant, owing to availability of high resolution measurement devices and improved computational methods.

As concrete application we have estimated the diffusivity in a stochastic Meinhardt model for cell repolarisation. For this model, we have demonstrated through simulations that moderate levels of dynamic noise do not destroy the pattern formation mechanism, but amplify it, leading to faster repolarisation and front splitting. This is achieved despite the simple activator-inhibitor structure of (1.1) and using only space-time white noise. We believe that this is the starting point for studying more detailed models for cell repolarisation based on SPDEs with spatially nonhomogeneous and possibly multiplicative noise. In this way we hope to obtain models that recover the variations within cells and between different cell populations better. The estimation methods developed here will be essential in calibrating these models to experimental data.

Appendix A. Proofs.

In the following, we consider for fixed $T < \infty$ a filtered probability space $(\Omega, \mathcal{F}, (\mathcal{F}_t)_{0\leqslant t\leqslant T}, \mathbb{P})$. Unless stated otherwise, all limits are taken as $\delta \to 0$. C always denotes a generic positive constant which may change from line to line. $A \lesssim B$ means $A \leqslant CB$ and $A_n = \mathcal{O}_{\mathbb{P}}(B_n)$ means that A_n/B_n is tight, that is, $\sup_n \mathbb{P}(|A_n| > C|B_n|) \to 0$ as $C \to \infty$. We also write $\Delta = \partial^2/\partial x^2$ to denote the Laplacian on $L^2(\Lambda) = L^2(\Lambda; \mathbb{R})$ with periodic boundary conditions.

A.1. Existence of a unique solution.

Reformulation and mild solution. Let us first reformulate the Meinhardt model as an SPDE in the space $L^2(\Lambda; \mathbb{R}^2)$. Let S_A and S_I denote the analytic and self-adjoint semigroups generated by $D_A\Delta$ and $D_I\Delta$ on $L^2(\Lambda)$. For smooth $z = (z_1, z_2) \in L^2(\Lambda; \mathbb{R}^2)$ consider also the differential operator $\mathcal{A}z = (D_A\Delta z_1, D_I\Delta z_2)$ with periodic boundary conditions, which generates the semigroup $S(t) = (S_A(t), S_I(t))$ on $L^2(\Lambda; \mathbb{R}^2)$. Let $B : L^2(\Lambda; \mathbb{R}^2) \to L^2(\Lambda; \mathbb{R}^2)$, $Bz = (\sigma_A z_1, \sigma_I z_2)$ and define $F : L^2(\Lambda; \mathbb{R}^2) \to L^2(\Lambda; \mathbb{R}^2)$ by

$$F(z)(x) = (F_A(z)(x), F_I(z)(x)) = (f_A(z(x), x), f_I(z(x), x)) .$$

Consider two independent cylindrical Wiener processes W_A, W_I on $L^2(\Lambda)$ such that $W(t) = (W_A(t), W_I(t))$ is a cylindrical Wiener process on $L^2(\Lambda; \mathbb{R}^2)$, and formally $dW(t) = (\xi_A(t), \xi_I(t))dt$. Solving (1.1) then corresponds to finding a solution $X = (A, I)$ to the SPDE

$$\begin{cases} dX(t) = (\mathcal{A}X(t) + F(X(t)))\, dt + B\, dW(t), \quad 0 < t \leqslant T, \\ X(0) = (A_0, I_0), \\ X(t, 0) = X(t, L), \quad 0 \leqslant t \leqslant T. \end{cases} \tag{A.1}$$

We use the mild solution concept of [12]. We will show that there exists a process X taking values in $L^2(\Lambda; \mathbb{R}^2)$ satisfying

$$X(t) = S(t)X(0) + \int_0^t S(t-s)F(X(s))ds + \int_0^t S(t-s)BdW(s). \tag{A.2}$$

Linear and nonlinear parts. The idea is to obtain the existence of X from $X := \bar{X} + \tilde{X}$ with $\bar{X}(t) := \int_0^t S(t-s)BdW(s)$ and where $\tilde{X}$ satisfies

$$\tilde{X}(t) = S(t)X(0) + \int_0^t S(t-s)F(\bar{X}(s) + \tilde{X}(s))ds, \quad 0 \leqslant t \leqslant T. \tag{A.3}$$

The process $\bar{X}$ is the unique mild solution to the linear SPDE (A.1) (with $F \equiv 0$ and $X(0) = 0$) and takes values in $L^2(\Lambda; \mathbb{R}^2)$ (apply, for example, [3, Proposition 30] separately to the component processes $\bar{A}$, $\bar{I}$). Finding a process $\tilde{X}$ solving (A.3), on the other hand, means equivalently finding a solution to the nonlinear PDE with random coefficients

$$\frac{\partial}{\partial t}\tilde{X}(t) = \mathcal{A}\tilde{X}(t) + F(\bar{X}(t) + \tilde{X}(t)), \quad 0 < t \leqslant T, \quad \tilde{X}(0) = X(0). \tag{A.4}$$

Since this equation does not depend explicitly on the noise process W anymore, it can be solved for a fixed realisation of $\bar{X}$. The proof follows from a classical fixed point argument.

Proof of Theorem 2.1. We will extend [3, Theorem 31] to the present situation, that is to a system of two equations and with periodic boundary conditions. For $s \in \mathbb{R}$, $p \geqslant 1$ and $u \in L^p(\Lambda)$ define the norm $\|u\|_{s,p} = \|(I-\Delta)^{s/2}u\|_{L^p(\Lambda)}$ and consider the Bessel potential spaces

$$W^{s,p}(\Lambda) = \{u \in L^p(\Lambda) : \|u\|_{s,p} < \infty\}.$$

Abusing notation, for $v \in L^p(\Lambda;\mathbb{R}^2)$ we also write $\|v\|_{s,p} = (\|v_1\|_{s,p}^2 + \|v_2\|_{s,p}^2)^{1/2}$ and define accordingly the spaces

$$W^{s,p}(\Lambda;\mathbb{R}^2) = \left\{v \in L^p(\Lambda;\mathbb{R}^2) : \|v\|_{s,p} < \infty\right\}.$$

Note that $I-\Delta$ is a strictly positive operator and thus $(I-\Delta)^{-1}$ is a bounded operator on $L^2(\Lambda)$ for periodic boundary conditions, while $(-\Delta)^{-1}$ is not. The spaces $W^{s,p}(\Lambda)$ differ from the classical Sobolev spaces, but allow for a Sobolev embedding theorem (see for example [10, Section 2.3]). The reader can check that the statement of [3, Theorem 31] remains true, once the spaces $W^{s,p}(\Lambda)$ appearing in that theorem are replaced by the spaces $W^{s,p}(\Lambda;\mathbb{R}^2)$ from above.

Let now $\eta < 2$ and $0 < s < 1/2$ such that $s+\eta > 2$, and fix $p \geqslant 2$ such that $s > 1/p$. We obtain from [3, Proposition 30] for $\Lambda = [0,L]$ that the linear process satisfies $\bar{X} \in C([0,T];W^{s,p}(\Lambda;\mathbb{R}^2))$. Since $X(0) \in C^{2+s}(\Lambda;\mathbb{R}^2)$ by assumption, after checking the assumptions on F in the aforementioned theorem, which we will do below, we can then conclude that $\tilde{X}$ satisfying (A.3) exists uniquely with $\tilde{X} \in C([0,T];W^{s+\eta,p}(\Lambda;\mathbb{R}^2))$. In particular, $X \in C([0,T];W^{s,p}(\Lambda;\mathbb{R}^2))$. The result follows from applying the Sobolev embedding theorem componentwise such that $\tilde{X} \in C([0,T];C^{2+s}(\Lambda;\mathbb{R}^2))$ and $X \in C([0,T];C^{s}(\Lambda;\mathbb{R}^2))$ for all $s < 1/2$, as claimed.

We are left with checking that F satisfies Assumptions $A_{s',\eta,p'}$, $L_{s,\eta,p}$ and $C_{s_1,s}$ from [3, Appendix B.2] for $s_1 = 0$ and all $s_1 \leqslant s' \leqslant s$, $2 \leqslant p' \leqslant p$. It is enough to check this separately for the component functions F_A, F_I. Since $z \mapsto F_I(z) = b_I z_1 - r_I z_2$ is linear, Assumptions $A_{s',\eta,p'}$ and $L_{s,\eta,p}$ follow immediately from choosing $\varepsilon = 2-\eta$, $h = C$ for a constant $C < \infty$, and using that $r \mapsto \|z_1\|_{r,p}$ is increasing. Moreover, assumption $C_{0,s}$ follows from the Cauchy-Schwarz inequality with b being the identity (up to a constant). With respect to F_A write

$$\begin{aligned} F_A(z)(x) &= r_A s(x) f_1(z_1(x)) f_2(z_2(x)) - r_A f_3(z_1(x)), \\ \text{with} \quad f_1(y) &= \frac{b_A + y^2}{1 + s_A y^2}, \quad f_2(y) = \frac{1}{s_I + |y|}, \quad f_3(y) = y, \quad y \in \mathbb{R}. \end{aligned}$$

Note that s and f_1 are bounded, smooth and have also bounded derivatives, while f_2 is bounded and Lipschitz. This already implies Assumption $C_{0,s}$. With respect to Assumption $A_{s',\eta,p'}$ let again $\varepsilon = 2-\eta$. We will show by interpolation, cf. [26], that

$$\|F_A(z)\|_{s',p'} \lesssim \|z\|_{s',p'}, \quad 0 \leqslant s' \leqslant 1, \quad z \in W^{s',p'}(\Lambda;\mathbb{R}^2). \tag{A.5}$$

Indeed, since the spaces $W^{s,p}(\Lambda)$ (and thus $W^{s,p}(\Lambda;\mathbb{R}^2)$) are compatible with complex

interpolation ([10, Section 2.2]), it is by [26, Theorem 2.1.6] enough to prove

$$\|F_A(z)\|_{0,p'} \lesssim \|z\|_{0,p'}, \quad z \in L^{p'}(\Lambda;\mathbb{R}^2),$$
$$\|F_A(z)\|_{1,p'} \lesssim \|z\|_{1,p'}, \quad z \in W^{1,p'}(\Lambda;\mathbb{R}^2).$$

The first inequality holds trivially, because $F_A + r_A f_3$ is bounded and f_3 is linear. For the second inequality we have

$$\|F_A(z)\|_{1,p'} \lesssim \|f_1'(z_1)\frac{\partial}{\partial x}z_1\|_{0,p'} + \|f_2'(z_2)\frac{\partial}{\partial x}z_2\|_{0,p'} + \|\frac{\partial}{\partial x}z_1\|_{0,p'} \lesssim \|z\|_{1,p'},$$

with weak derivatives f_1', f_2', proving Assumption $A_{s',\eta,p'}$. At last, for Assumption $L_{s,\eta,p}$ observe that $W^{s,p}(\Lambda)$ is a Banach algebra with respect to pointwise multiplication when $s > 1/p$ (proof analogous to [1, Theorem 4.39]). Hence we compute for $u, v \in W^{s,p}(\Lambda;\mathbb{R}^2)$

$$\begin{aligned}\|F_A(u) - F_A(v)\|_{s,p} &\lesssim \|f_1(u_1)f_2(u_2) - f_1(v_1)f_2(v_2)\|_{s,p} + \|u_1 - v_1\|_{s,p}\\ &\lesssim \|f_2(u_2)\|_{s,p}\|f_1(u_1) - f_1(v_1)\|_{s,p} + \|f_1(v_1)\|_{s,p}\|f_2(u_1) - f_2(v_1)\|_{s,p}\\ &\quad + \|u_1 - v_1\|_{s,p} \lesssim \|u - v\|_{s,p},\end{aligned}$$

concluding in the last line by (A.5) and [3, Lemma 38(ii)] applied to f_1, f_2. ∎

A.2. Results on parameter estimation. Since we are not considering Dirichlet boundary conditions, we cannot rely on the Feynman-Kac arguments of [4] and [3] to study the action of the semigroup generated by Δ on K_{δ,x_k}. The following proof avoids this issue, and also holds for more general boundary conditions. The proof is inspired by [3, Theorem 3], but is fully self-contained.

Consider the decomposition $A = \bar{A} + \tilde{A}$ into linear and nonlinear parts $\bar{A}$ and $\tilde{A}$ according to Section A.1. With this we also set

$$\begin{aligned}\bar{A}_\delta^\Delta(t,x_k) &:= \langle \bar{A}(t), \Delta K_{\delta,x_k}\rangle = \sigma_A \left\langle \int_0^t S_A(t-s)dW_A(s), \Delta K_{\delta,x_k}\right\rangle \\ &= \sigma_A \int_0^t \langle S_A(t-s)\Delta K_{\delta,x_k}, dW_A(s)\rangle,\end{aligned} \tag{A.6}$$

as well as $\tilde{A}_\delta^\Delta(t,x_k) = \langle \tilde{A}(t), \Delta K_{\delta,x_k}\rangle$. We also use the linear observed Fisher information $\bar{\mathcal{I}}_\delta = \sum_{k=1}^M \int_0^T \left(\bar{A}_\delta^\Delta(t,x_k)\right)^2 dt$.

Proof of Theorem 4.1. Using that $\|K_{\delta,x_k}\| = \|K\|_{L^2(\mathbb{R})}$, the basic error decomposition (4.5) can equivalently be written as

$$\delta^{-1}(\hat{D}_{A,\delta} - D_A) = (\delta^2\mathcal{I}_\delta)^{-1}\delta R_\delta + \sigma_A\|K\|_{L^2(\mathbb{R})}(\delta^2\mathcal{I}_\delta)^{-1/2}(\mathcal{I}_\delta^{-1/2}M_\delta).$$

The martingale part satisfies $M_\delta = M_\delta(T)$, where $M_\delta(t') = \sum_{k=1}^M \int_0^{t'} A_\delta^\Delta(t,x_k)dW_k(t)$ is a continuous martingale in $t' \geqslant 0$ with respect to the natural filtration generated by the Brownian motions W_k as a sum of such martingales. Without loss of generality let the K_{δ,x_k} have disjoint supports, which is true for sufficiently small δ, since M is fixed. But then the

processes W_k are independent and the quadratic variation of the martingale $M_\delta(t')$ at $t'=T$ is exactly $\mathcal{I}_\delta$. By a classical time-change [20, Theorem 3.4.6] we can write $M_\delta = \bar{w}_{\mathcal{I}_\delta}$ for a Brownian motion $\bar{w}$, possibly defined on an extension of the underlying probability space. We conclude from Proposition A.1(i,ii,iii) that $\mathcal{I}_\delta / \mathbb{E}[\bar{\mathcal{I}}_\delta] \to 1$ in probability and

$$\frac{M_\delta}{\mathcal{I}_\delta^{1/2}} = \frac{\mathbb{E}[\bar{\mathcal{I}}_\delta]^{1/2}}{\mathcal{I}_\delta^{1/2}} \cdot \frac{\bar{w}_{\mathcal{I}_\delta}}{\mathbb{E}[\bar{\mathcal{I}}_\delta]^{1/2}} \xrightarrow{d} \mathcal{N}(0,1).$$

Proposition A.1(i,ii,iii) also shows $\delta^2 \mathcal{I}_\delta \to \kappa$ in probability and the result follows from Slutsky's Lemma and Proposition A.1(iv). ∎

Proposition A.1. *The following holds as $\delta \to 0$:*
(i) $\delta^2 \mathbb{E}[\bar{\mathcal{I}}_\delta] \to \kappa := MT\sigma_A^2 D_A^{-1} \|K\|^2_{L^2(\mathbb{R})} \Sigma^{-1}$ *with Σ from Theorem 4.1,*
(ii) $\bar{\mathcal{I}}_\delta / \mathbb{E}[\bar{\mathcal{I}}_\delta] \to 1$ *in probability,*
(iii) $\mathcal{I}_\delta = \bar{\mathcal{I}}_\delta + \mathcal{O}_{\mathbb{P}}(\delta^{-1/2})$,
(iv) $R_\delta = \mathcal{O}_{\mathbb{P}}(\delta^{-1/2})$.

Proof. (i). We find from (A.6) and Itô's isometry ([12, Proposition 4.28]) that

$$\mathbb{E}[\bar{\mathcal{I}}_\delta] = \sigma_A^2 \sum_{k=1}^M \int_0^T \int_0^t \|S_A(s) \Delta K_{\delta,x_k}\|^2 ds dt. \tag{A.7}$$

The operators $S_1(s)$ are self-adjoint such that $\|S_A(s)\Delta K_{\delta,x_k}\|^2 = \langle S_A(2s)\Delta K_{\delta,x_k}, \Delta K_{\delta,x_k}\rangle$. The semigroup identity $2\int_0^t S_A(2s) D_A \Delta K_{\delta,x_k} ds = S_A(2t) K_{\delta,x_k} - K_{\delta,x_k}$ therefore implies

$$\begin{aligned}
\mathbb{E}[\bar{\mathcal{I}}_\delta] &= \frac{1}{2} D_A^{-1} \sigma_A^2 \sum_{k=1}^M \left(\int_0^T \langle S_A(2t)\Delta K_{\delta,x_k}, K_{\delta,x_k}\rangle dt - T\langle K_{\delta,x_k}, \Delta K_{\delta,x_k}\rangle \right) \\
&= \frac{1}{2} D_A^{-1} \sigma_A^2 \sum_{k=1}^M \left(\frac{1}{2} D_A^{-1} \langle S_A(2T) K_{\delta,x_k} - K_{\delta,x_k}, K_{\delta,x_k}\rangle - T\langle K_{\delta,x_k}, \Delta K_{\delta,x_k}\rangle \right).
\end{aligned}$$

Noting that $\|S_A(T)K_{\delta,x_k}\| \leqslant \|K_{\delta,x_k}\|$, because the semigroup is contractive, (i) follows from $\langle K_{\delta,x_k}, \Delta K_{\delta,x_k}\rangle = -\delta^{-2} \|\frac{\partial}{\partial x} K\|^2_{L^2(\mathbb{R})}$.

(ii). It is enough to show $\delta^4 \mathrm{Var}(\bar{\mathcal{I}}_\delta) \to 0$, because this and (i) imply $\mathrm{Var}(\bar{\mathcal{I}}_\delta)/\mathbb{E}[\bar{\mathcal{I}}_\delta]^2 \to 0$. Since M is fixed, we can use the Cauchy-Schwarz inequality to obtain the upper bound $\mathrm{Var}(\bar{\mathcal{I}}_\delta) \leqslant M \sum_{k=1}^M \mathrm{Var}(\int_0^T (\bar{A}_\delta^\Delta(t,x_k))^2 dt)$. (A.6) shows that the $\bar{A}_\delta^\Delta(t,x_k)$ are centered Gaussian random variables. Wick's formula ([18, Theorem 1.28]) gives

$$\begin{aligned}
\mathrm{Var}(\bar{\mathcal{I}}_\delta) &\lesssim \sum_{k=1}^M \int_0^T \int_0^T \mathrm{Cov}\left(\left(\bar{A}_\delta^\Delta(t,x_k)\right)^2, \left(\bar{A}_\delta^\Delta(t',x_k)\right)^2 \right) dt' dt \\
&= 4 \sum_{k=1}^M \int_0^T \int_0^t \mathrm{Cov}\left(\bar{A}_\delta^\Delta(t,x_k), \bar{A}_\delta^\Delta(t',x_k)\right)^2 dt' dt \\
&= 4\sigma_A^4 \sum_{k=1}^M \int_0^T \int_0^t \left(\int_0^{t'} \langle S_A(t-s)\Delta K_{\delta,x_k}, S_A(t'-s)\Delta K_{\delta,x_k}\rangle ds \right)^2 dt' dt,
\end{aligned}$$

again using Itô's isometry in the last line. Arguing as in (i) by the semigroup identity and $S_A(t-s) = S_A(t-t')S_A(t'-s)$, the ds-integral equals

$$\int_0^{t'} \langle S_A(2(t'-s))\Delta K_{\delta,x_k}, S_A(t-t')\Delta K_{\delta,x_k}\rangle ds$$
$$= \frac{1}{2D_A}\langle (S_A(2t')-I)K_{\delta,x_k}, S_A(t-t')\Delta K_{\delta,x_k}\rangle \leqslant \frac{1}{2D_A}\langle K_{\delta,x_k}, S_A(t-t')(-\Delta)K_{\delta,x_k}\rangle,$$

where we used in the inequality that the $-\Delta$ and thus $S_A(t)$ for $t \geqslant 0$ are self-adjoint, non-negative operators, which commute. This also shows that the ds-integral from above is in fact non-negative, and so we obtain from the last display using the Cauchy-Schwarz inequality

$$\mathrm{Var}(\bar{\mathcal{I}}_\delta) \lesssim \|K\|^2_{L^2(\mathbb{R})} \sum_{k=1}^M \int_0^T \int_0^t \|S_A(t')\Delta K_{\delta,x_k}\|^2 dt'dt \lesssim \mathbb{E}[\bar{\mathcal{I}}_\delta] \lesssim \delta^{-2},$$

cf. (A.7) and (i), implying $\delta^4 \mathrm{Var}(\bar{\mathcal{I}}_\delta) \to 0$ and (ii) follows.

(iii). Recall from the proof of Theorem 2.1 that $\tilde{A} \in C([0,T]; C^2(\Lambda))$ $\mathbb{P}$-almost surely. This means

$$\left|\tilde{A}^\Delta_\delta(t,x_k)\right| = \left|\langle \Delta\tilde{A}(t), K_{\delta,x_k}\rangle\right| \leqslant \|\tilde{A}\|_{C([0,T];C^2(\Lambda))}\|K_{\delta,x_k}\|_{L^1(\Lambda)} = \mathcal{O}_{\mathbb{P}}(\delta^{1/2}), \tag{A.8}$$

using $\|K_{\delta,x_k}\|_{L^1(\Lambda)} \leqslant \delta^{1/2}\|K\|_{L^1(\mathbb{R})}$. We conclude by the Cauchy-Schwarz inequality and (i), because

$$\left|\mathcal{I}_\delta - \bar{\mathcal{I}}_\delta\right| \lesssim \sum_{k=1}^M \int_0^T \left(\left(\tilde{A}^\Delta_\delta(t,x_k)\right)^2 + 2\left|\tilde{A}^\Delta_\delta(t,x_k)\bar{A}^\Delta_\delta(t,x_k)\right|\right) dt = \mathcal{O}_{\mathbb{P}}(\delta + \delta^{1/2}\bar{\mathcal{I}}_\delta^{1/2}).$$

(iv). The Cauchy-Schwarz inequality and (i,ii,iii) show

$$|R_\delta| \lesssim \mathcal{I}_\delta^{1/2}\left(\sum_{k=1}^M \int_0^T \langle F_A(X(t)), K_{\delta,x_k}\rangle^2 dt\right)^{1/2} \lesssim \mathcal{I}_\delta^{1/2}\delta^{1/2}\|F_A(X(\cdot))\|_{C([0,T];C(\Lambda))}\|K\|_{L^1(\mathbb{R})}.$$

This is of order $\mathcal{O}_{\mathbb{P}}(\delta^{-1/2})$, using that $F_A(X(\cdot)) \in C([0,T];C(\Lambda))$ $\mathbb{P}$-almost surely by Theorem 2.1, recalling that $z \mapsto F_A(z)$ is Lipschitz, and the result follows. ∎

Appendix B. Setup of numerical and real data experiments.

All simulations were performed with parameters and initial conditions obtained by calibrating the deterministic Meinhardt model to experimental data. The parameters in (1.1), (2.1) and (2.2) are taken from [24, Table S1, Figure 4],

$$\begin{aligned} D_A &= 4.415 \times 10^{-2}, & D_I &= 9.768 \times 10^{-2}, \\ r_A &= 2.393 \times 10^{-1}, & r_I &= 2.378 \times 10^{-1}, \\ b_A &= 2.776 \times 10^{-1}, & b_I &= 2.076 \times 10^{-1}, \\ s_A &= 5.647 \times 10^{-3}, & s_I &= 3.397 \times 10^{-1}, \\ a &= 1.280 \times 10^{-2}. \end{aligned}$$

The initial conditions for the activator A and inhibitor I are taken correspondingly from [24, Table S2, Figure 4].

Numerical simulations were performed in the programming language Julia using a finite difference scheme for semilinear SPDEs [25]. The source code can be obtained from the authors upon request. For comparison to the experimental setup of [24] we consider $T = 100$, $L = 20$ and choose $dt = T/N$ and $dx = L/M$ as step sizes for time and space discretisations, such that the Courant-Friedrichs-Lewy (CFL) condition is satisfied, ensuring stable simulations, that is $dt \asymp (dx)^2$ [25].

References.

[1] Adams, R. and Fournier, J. (2003). *Sobolev Spaces*. Elsevier Science.

[2] Alonso, S., Stange, M., and Beta, C. (2018). Modeling random crawling, membrane deformation and intracellular polarity of motile amoeboid cells. *PLOS ONE*, 13(8):e0201977.

[3] Altmeyer, R., Cialenco, I., and Pasemann, G. (2020). Parameter estimation for semilinear spdes from local measurements. *arXiv preprint arXiv:2004.14728*.

[4] Altmeyer, R. and Reiß, M. (2020). Nonparametric estimation for linear SPDEs from local measurements. *Annals of Applied Probability, to appear*.

[5] Bibinger, M. and Trabs, M. (2020). Volatility estimation for stochastic PDEs using high-frequency observations. *Stochastic Processes and their Applications*, 130(5):3005–3052.

[6] Cheng, Y., Felix, B., and Othmer, H. G. (2020). The roles of signaling in cytoskeletal changes, random movement, direction-sensing and polarization of eukaryotic cells. *Cells*, 9(6):1437.

[7] Chong, C. (2020). High-frequency analysis of parabolic stochastic PDEs. *Annals of Statistics, to appear*.

[8] Cialenco, I. (2018). Statistical inference for SPDEs: an overview. *Statistical Inference for Stochastic Processes*, 21(2):309–329.

[9] Cialenco, I. and Huang, Y. (2019). A note on parameter estimation for discretely sampled SPDEs. *Stochastics and Dynamics*, 24:2050016.

[10] Cirant, M. and Goffi, A. (2019). On the existence and uniqueness of solutions to time-dependent fractional mfg. *SIAM Journal on Mathematical Analysis*, 51(2):913–954.

[11] Cramer, L. P. (2013). Mechanism of cell rear retraction in migrating cells. *Current opinion in cell biology*, 25(5):591–599.

[12] Da Prato, G. and Zabczyk, J. (2014). *Stochastic equations in infinite dimensions*. Cambridge university press.

[13] Dalous, J., Burghardt, E., Müller-Taubenberger, A., Bruckert, F., Gerisch, G., and Bretschneider, T. (2008). Reversal of cell polarity and actin-myosin cytoskeleton reorganization under mechanical and chemical stimulation. *Biophysical journal*, 94(3):1063–1074.

[14] Evans, L. C. (2010). *Partial Differential Equations*. American Mathematical Soc.

[15] Hairer, M. (2009). An Introduction to Stochastic PDEs. *arXiv preprint arXiv:0907.4178*.

[16] Hildebrandt, F. and Trabs, M. (2019). Parameter estimation for SPDEs based on

discrete observations in time and space. *arXiv preprint arXiv:1710.01649*.

[17] Huebner, M. and Rozovskii, B. (1995). On asymptotic properties of maximum likelihood estimators for parabolic stochastic PDE's. *Probability Theory and Related Fields*, 103(2):143–163.

[18] Janson, S. (1997). *Gaussian Hilbert Spaces*. Cambridge University Press.

[19] Jilkine, A. and Edelstein-Keshet, L. (2011). A comparison of mathematical models for polarization of single eukaryotic cells in response to guided cues. *PLoS Comput Biol*, 7(4):e1001121.

[20] Karatzas, I. and Shreve, S. (1998). *Brownian Motion and Stochastic Calculus*. Springer.

[21] Levchenko, A. and Iglesias, P. A. (2002). Models of eukaryotic gradient sensing: application to chemotaxis of amoebae and neutrophils. *Biophysical journal*, 82(1):50–63.

[22] Liptser, R. and Shiryaev, A. (2001). *Statistics of Random Processes I.* General Theory. Springer.

[23] Lockley, R. (2017). *Image-based Modelling of Cell Reorientation*. PhD thesis, University of Warwick.

[24] Lockley, R., Ladds, G., and Bretschneider, T. (2015). Image based validation of dynamical models for cell reorientation. *Cytometry Part A*, 87(6):471–480.

[25] Lord, G. J., Powell, C. E., and Shardlow, T. (2014). *An Introduction to Computational Stochastic PDEs*. Cambridge University Press.

[26] Lunardi, A. (2009). *Interpolation theory*. Edizioni della Normale.

[27] Meinhardt, H. (1999). Orientation of chemotactic cells and growth cones: models and mechanisms. *Journal of cell science*, 112(17):2867–2874.

[28] Meinhardt, H. (2009). *The algorithmic beauty of sea shells*. Springer.

[29] Mullins, R. D., Heuser, J. A., and Pollard, T. D. (1998). The interaction of arp2/3 complex with actin: nucleation, high affinity pointed end capping, and formation of branching networks of filaments. *Proceedings of the National Academy of Sciences*, 95(11):6181–6186.

[30] Otsuji, M., Ishihara, S., Kaibuchi, K., Mochizuki, A., and Kuroda, S. (2007). A mass conserved reaction-diffusion system captures properties of cell polarity. *PLoS Comput Biol*, 3(6):p. e108.

[31] Pasemann, G., Flemming, S., Alonso, S., Beta, C., and Stannat, W. (2020). Diffusivity estimation for activator-inhibitor models: Theory and application to intracellular dynamics of the actin cytoskeleton. *arXiv preprint arXiv:2005.09421*.

[32] Pasemann, G. and Stannat, W. (2020). Drift estimation for stochastic reaction-diffusion systems. *Electronic Journal of Statistics*, 14(1):547–579.

[33] Spill, F., Guerrero, P., Alarcon, T., Maini, P. K., and Byrne, H. (2015). Hybrid approaches for multiple-species stochastic reaction–diffusion models. *Journal of computational physics*, 299:429–445.

[34] Turing, A. M. (1952). The chemical basis of morphogenesis. *Philosophical Transactions of the Royal Society of London. Series B, Biological Sciences*, 237(641):37–72.